Inorganic Chemistry Communications 175 (2025) 114160

Contents lists available at ScienceDirect

Inorganic Chemistry Communications

journal homepage: www.elsevier.com/locate/inoche

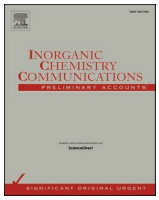

Research Article

Cationic dye adsorption on the bioadsorbents based on chitosan and sodium alginate-iron oxide nanoparticles: Kinetic, isotherm and thermodynamic studies

Umran Duru Kamaci [a,*], Musa Kamaci [b]

[a] Faculty of Arts and Sciences, Department of Chemistry, Yildiz Technical University, Esenler 34220 Istanbul, Turkey
[b] Piri Reis University, Tuzla 34940, Istanbul, Turkey

ARTICLE INFO

Keywords:
Nanoparticles
Methylene blue
Iron oxide
Adsorption
Chitosan

ABSTRACT

Herein, we fabricated a series of bioadsorbents based on chitosan and sodium alginate-iron oxide nanoparticles for the adsorption of methylene blue. As known, iron nanoparticle-based bioadsorbents have exhibited outstanding adsorption behavior while chitosan has been shown low adsorption due to its low surface area. For this reason, we aimed to increase the chitosan s surface area and dye adsorption behavior by mixing it with sodium alginate and iron nanoparticles. Some characterization techniques such as Fourier Transform-Infrared Spectroscopy (FT-IR), X-ray diffraction (XRD), Scanning Electron Microscopy (SEM), Brunauer-Emmett-Teller (BET), and thermogravimetric (TG) analysis were used to confirm the structure of bioadsorbents and to investigate crystalline, surface, and thermal properties. The adsorption of methylene blue onto the bioadsorbents was fitted to pseudo-second order kinetic and Langmuir isotherm models. The maximum methylene blue adsorption capacity was found between 162.77 and 212.77 mg/g. Moreover, thermodynamic parameters such as change in free energy (ΔG^o, in the range from −4. 524 to −0.748 kJ/mol), change in enthalpy (ΔH^o, in the range from −31.100 to −28.894 kJ/mol), and change in entropy (ΔS^o, in the range from −90.963 to −84.454 kJ mol^{-1} K^{-1}) were calculated with negative values. The findings from the thermodynamic studies indicated that the adsorption process was spontaneous and exothermic.

1. Introduction

Recently, the use of metal-based nanomaterials such as nanoparticles, nanotubes, bioadsorbents, and nanofibers for the adsorption of organic pollutants and dyes in the aquatic environment has become promising [1]. Different types of metal-based nanomaterials such as aluminum (Al), copper (Co), gold (Au), iron (Fe), and titanium (Ti) were fabricated and used for the adsorption of pollutants [2]. One of the most important classes of these nanomaterials is iron oxide nanoparticles due to the low cost of iron, which is the second most abundant element on earth [3]. In addition, iron-based nanoparticles have exhibited some superior properties such as high adsorption capacity, reactivity, and biocompatibility as well as chemical, thermal, and mechanical stability [4].

Bioadsorbents have been obtained among nanomaterial types by combining natural biopolymers with metal or metal nanoparticles [5]. Moreover, biopolymers and their derivatives containing chitosan, starch, sodium alginate, and pullulan have been generally used to fabricate the bioadsorbents [6–8]. Chitosan is one of the most bountiful polymers in nature, and it is a hydrophilic polymer obtained via the deacetylation of chitin [9,10]. This natural polymer is composed of large amounts of hydroxyl (–OH) and amine ($–NH_2$) groups in its structure [11]. Chitosan and its derivatives can easily create active sites in their structures due to the presence of these functional groups [12]. Due to these properties, it is widely used as a bioadsorbent in the removal of pollutants and heavy metal ions in water by chelating or using the adsorption method [13,14]. On the other hand, the dye adsorption behavior of the chitosan-based adsorbents varies depending on some physicochemical properties such as pore size and specific surface area. Chitosan has also shown a low dye adsorption performance, and limited reusability due to its very low specific surface area [15]. Therefore, there is a need to develop chitosan adsorbents that are porous and have a high specific surface area.

To our knowledge, the literature has not reported chitosan

* Corresponding author.
E-mail address: umranduru@gmail.com (U.D. Kamaci).

https://doi.org/10.1016/j.inoche.2025.114160
Received 7 December 2024; Received in revised form 30 January 2025; Accepted 18 February 2025
Available online 21 February 2025

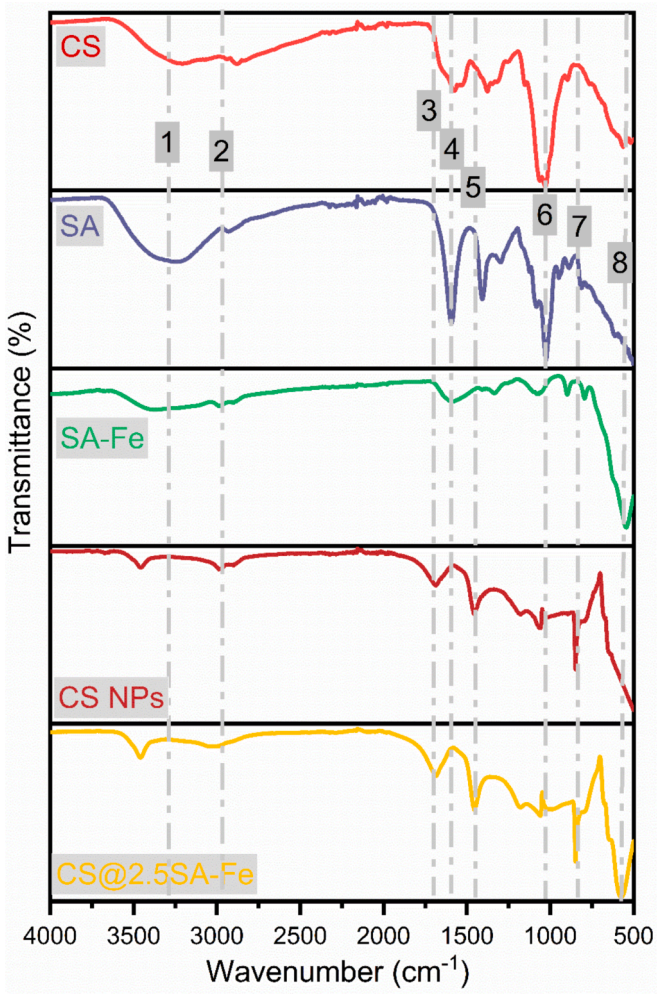

Fig. 1. FT-IR spectra of chitosan (CS), sodium alginate (SA), sodium alginate-iron nanoparticles (SA-Fe), chitosan nanoparticles (CS NPs), and chitosan nanoparticles containing 2.5 % sodium alginate-iron (CS@SA_Fe). (Stretching vibrations = 1: hydroxyl (–OH)/amine (–NH_2), 2: aliphatic –CH, 3: –NH, 4: symmetric –C═O, 5: anti-symmetric –C═O, 6: carboxylate anion (–C═O-O), 7: –C–O–C, and 8: Fe-O).

nanoparticles containing sodium alginate and iron oxide for methylene blue adsorption [16–18]. Moreover, we aimed to increase the chitosan's surface area and dye adsorption capacity. For this purpose, sodium alginate and iron oxide (SA_Fe) particles were prepared via the co-precipitation method. Then, these fabricated particles were mixed with chitosan to obtain novel bioadsorbents for the adsorption of methylene blue (MB). As known, MB is a heterocyclic aromatic compound classified as a cationic dye. It is used in different industries such as pharmaceuticals, dyes, textiles, pesticides, etc. Large amounts of MB have a negative impact on human health and can cause high blood pressure, mental disorders, and nausea because of its toxic structure [19]. The structural confirmation of the SA_Fe nanoparticles and bioadsorbents was carried out by using an FT-IR spectrometer. Morphological and thermal behaviors were investigated by using SEM and TG analysis techniques. Crystalline structure and surface area were clarified using XRD and BET analysis. The dye adsorption performance of the bioadsorbents was also optimized in terms of temperature, pH, bioadsorbent amounts, and contact time. Kinetics and isotherm experiments for the adsorption of methylene blue onto the bioadsorbent were also performed and thermodynamic parameters were calculated.

2. Material and methods

2.1. Reagents

Chitosan (CS, medium molecular weight, 75–85 % deacetylated), sodium alginate from brown algae (medium viscosity), iron (II) chloride tetrahydrate (Fe^{2+}, $FeCl_2{\cdot}4H_2O$, Mw. 198.81 g mol^{-1}), iron (III) chloride hexahydrate (Fe^{3+}, $FeCl_2{\cdot}6H_2O$, Mw. 270.30 g mol^{-1}), sodium hydroxide (NaOH, Mw. 40.00 g mol^{-1}), methylene blue (MB, Mw. 319.85 g mol^{-1}), and acetic acid (CH_3COOH, Mw. 60.05 g mol^{-1}) were purchased from Sigma Aldrich, and they were used without purification processes.

2.2. Synthesis of sodium alginate-iron oxide particles (SA_Fe)

The sodium alginate-iron oxide particles were prepared via the co-precipitation method as the following procedure [20]:

0.3 g of sodium alginate was dissolved in 30 mL of deionized water. After the sodium alginate was completely dissolved, the freshly prepared 50 mL of 1 M Fe^{2+}, and 50 mL of 2 M Fe^{3+} solutions were added into the sodium alginate matrix drop by drop. The mixture was stirred for 2 h at ambient conditions. Then, the sodium alginate-iron oxide mixture was precipitated by using a sodium hydroxide solution (25 %, w:v), and filtered. Particles were washed with distilled water (2x50 mL) and dried in a vacuum oven at around 65 °C.

2.3. Fabrication of the bioadsorbents

Chitosan (CS) and sodium alginate-iron oxide (SA_Fe) nanoparticles were prepared as the ionoprotic procedure, and they were abbreviated as CS, CS@2.5SA_Fe, CS@5.0SA_Fe, and CS@10.0SA_Fe according to the SA_Fe amount:

0.5 g of CS was weighed and dissolved in 25 mL of deionized water containing 2 % acetic acid. After obtaining a homogeneous solution, the SA_Fe nanoparticles in various amounts (2.5, 5.0, and 10.0 % of the total CS mass) were added to the chitosan solution, and the mixture was stirred at room temperature for 2 h. Then, the mixture was taken into a 5 mL syringe, added to the NaOH solution drop by drop to precipitate, and kept in this solution overnight. Finally, the bioadsorbents were filtered, washed several times with distilled water, and dried in an oven at around 70 °C [21,22].

2.4. Structural characterization

The structural characterization of the SA_Fe particles and bioadsorbents was performed by using Perkin-Elmer Spectrum Two Fourier Transform-Infrared spectrometer (FT-IR) with ATR unit in the range from 500 to 4000 cm^{-1}. The surface morphology was clarified by Zeiss EVO LS 10 Scanning Electron Microscopy (SEM) with the operating electron voltage of 10 kV, and the SA_Fe particles and bioadsorbents were coated with gold to obtain better microimages in these measurements. The crystalline nature of SA_Fe particles and bioadsorbents was detected via an X-Ray Powder Diffractometer (XRD) with a CuKα source. The specific surface area of the SA_Fe particles and bioadsorbents was analyzed by measuring the nitrogen adsorption and desorption isotherms using Barrett-Joyner-Halenda (BJH), and Brunauer-Emmett-Teller (BET). These measurements were carried out by using Micromeritics Asap 2020 – Quantachrome Quadrosorb SI. The thermal behavior and stability of the SA_Fe particles and bioadsorbents were investigated using a Perkin-Elmer Diamond Thermogravimetric analysis in the range from 20 and 700 ∘C under a nitrogen atmosphere with a heating rate of 10 °C min^{-1}.

2.5. Methylene blue adsorption

Methylene blue adsorption of CS, CS@2.5SA_Fe, CS@5.0SA_Fe, and

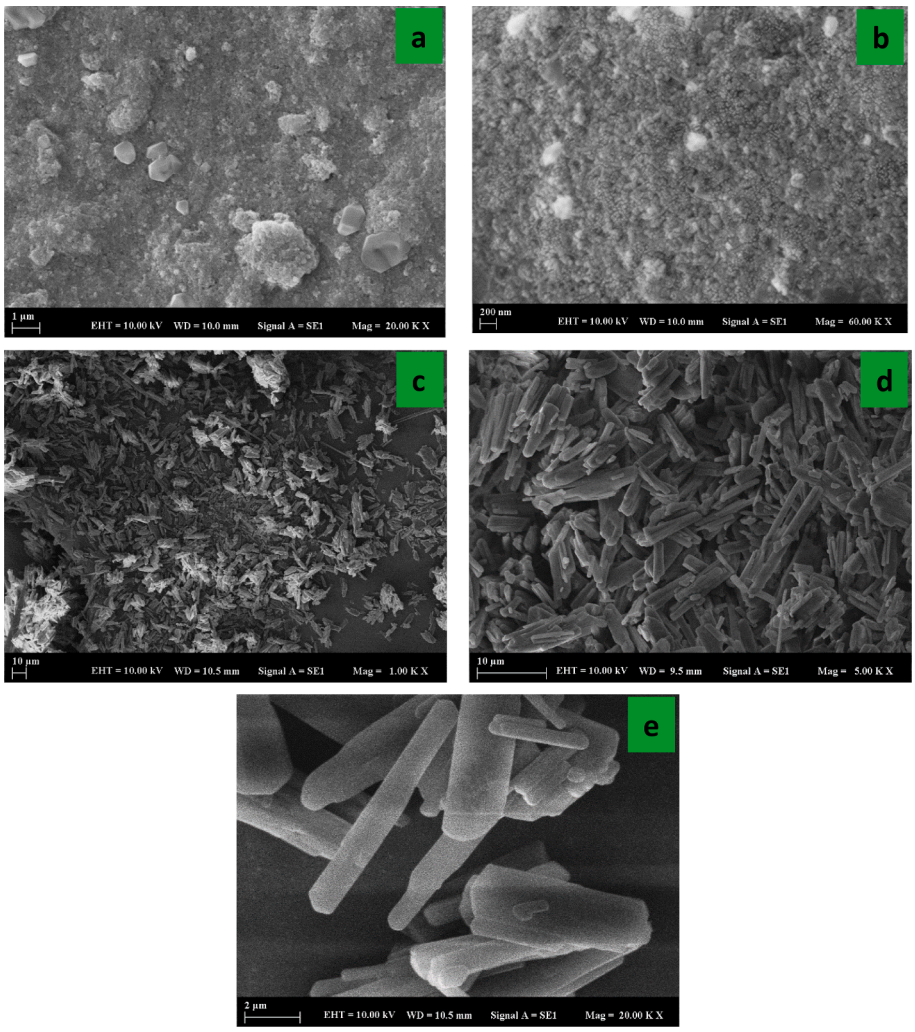

Fig. 2. SEM image of SA_Fe (a, b) and chitosan@5.0SA_Fe (c, d, e) nanoparticles at different magnitudes 1, 5, and 20 kX.

CS@10.0SA_Fe was measured using the batch experiment method. This experiment was carried out to compare the methylene blue adsorption efficiencies of the bioadsorbents from an aqueous environment. Also, the different adsorption parameters effects such as the reaction temperature (ranging from 20 to 60 °C), the pH of the dye solution (varying from 3 to 9), the contact time (ranging from 0 to 120 min), and the amounts of the bioadsorbent (ranging from 0 to 100 mg) were clarified on the adsorption capacity of the bioadsorbents.

In general terms, a certain amount of bioadsorbent was placed into the Erlenmeyer flask containing 50 mL of dye solution (20 mg L^{-1}). This mixture was stirred using a shaker for 2 h at 240 rpm. Then, the solution concentration was measured at 664 nm using a UV–Vis spectrophotometer, and the % dye removal efficiency and adsorption capacity (q_e) of the bioadsorbents were calculated with the help of the following equations [23]:

$$\%\,\text{Removal} = \frac{C_o - C_e}{C_o} \text{x}\, 100 \tag{1}$$

where C_o is the methylene blue concentration at the initial state (mg L^{-1}), and C_e is the dye concentration after the adsorption (mg L^{-1}).

$$\text{qe} = \frac{C_o - C_e}{m} \text{x}\, \text{V} \tag{2}$$

where qe is the dye equilibrium adsorption capacity (mg g^{-1}), m is the bioadsorbent amount (mg), and V is the volume of dye solution (50 mL).

2.6. Kinetics and thermodynamics

The pseudo-first and second-order kinetic models were used in the presence of a 20 mL dye stock solution (20 mg L^{-1}) at 293, 313, and 333 K, and the methylene blue adsorption efficiency of the bioadsorbents was clarified as a function of time.

The pseudo-first-order kinetic model [24]

$$ln(q_e - q_t) = -k_1 t + lnq_e \tag{3}$$

The pseudo-second-order kinetic model [25]

$$\frac{t}{q_t} = \frac{1}{k_2 q_e^2} + \frac{t}{q_e} \tag{4}$$

where k_1 is the rate constant for the first-order kinetic model (min^{-1}), and k_2 is the rate constant for the second-order kinetic model (g mg^{-1} min^{-1}).

Also, the Langmuir and Freundlich isotherm models were used to investigate the adsorption capacity of the CS, CS@2.5SA_Fe, CS@5.0SA_Fe, and CS@10.0SA_Fe in the presence of 10 mg bioadsorbents in the different initial dye concentration varying from 0 to 100 mg L^{-1} and temperature ranging from to 293 to 333 K.

The Freundlich isotherm [26]

$$\text{lnq}_e = \text{lnK}_F + \frac{1}{n}\text{lnC}_e \tag{5}$$

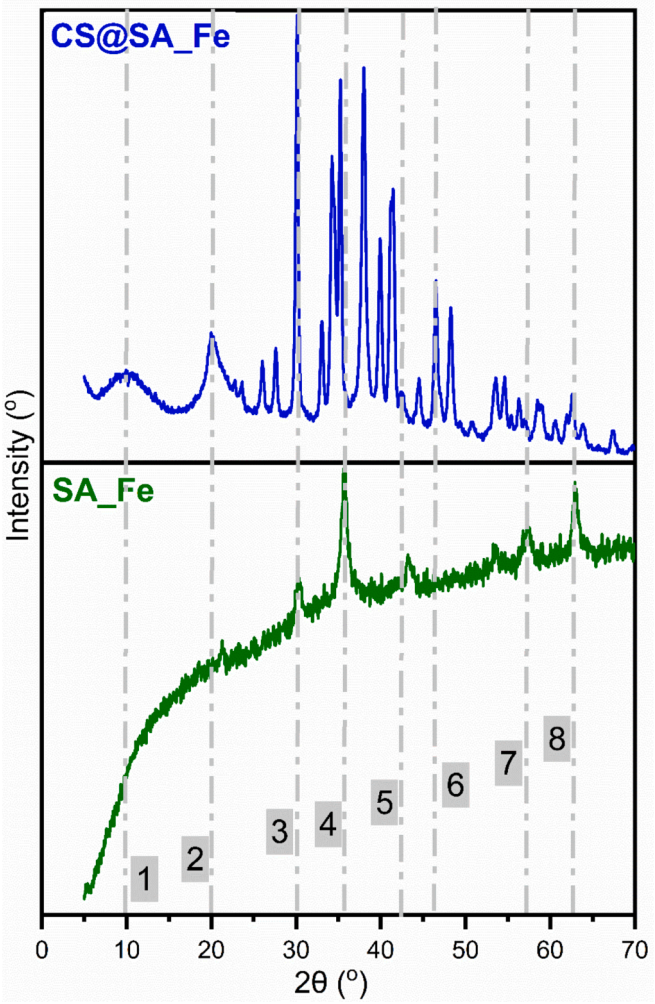

Fig. 3. XRD pattern of SA-Fe, and CS@SA-Fe nanoparticles.

The Langmuir isotherm [27]

$$\frac{C_e}{q_e} = \frac{1}{K_L.q_{max}} + \frac{C_e}{q_{max}} \quad (6)$$

where q_{max} is the maximum dye adsorption capacity of the bio-adsorbents (g/mg), K_F is the Freundlich adsorption constant ((mg/g) (L/mg)$^{1/n}$), K_L is the Langmuir adsorption constant (L/mg), and n is the adsorption intensity.

The basic thermodynamic parameters such as standard free energy (G°), enthalpy (H°), and entropy (S°) were evaluated by fitting to the following Eqs. (7), and 8 [23]:

$$\Delta G^{\circ} = -RT\ln K_L \quad (7)$$

$$lnK_L = \frac{\Delta S^{\circ}}{R} - \frac{\Delta H^{\circ}}{RT} \quad (8)$$

where ΔG°, ΔH°, and ΔS° are the changes in free energy (kJ/mol), enthalpy (kJ/mol), and entropy (kJ/mol), respectively. K_L is the Langmuir adsorption constant (L/mg), T is the absolute temperature (K), and R is the gas constant (8.314 J mol^{-1} K^{-1}), respectively.

3. Results and discussion

3.1. FT-IR analysis

To confirm the structure of the SA_Fe particles and bioadsorbents,

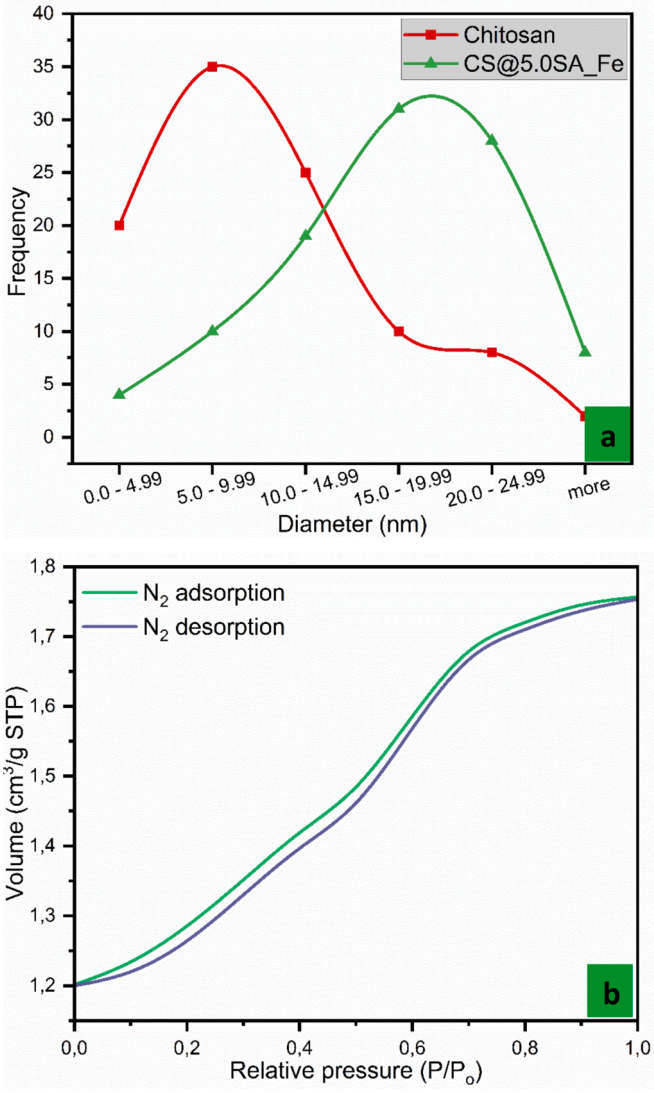

Fig. 4. Pore size distribution of chitosan and CS@5.0SA_Fe (a) and BET analysis of CS@5.0SA_Fe (b).

Fourier Transform-Infrared (FT-IR) analysis was performed (Fig. 1). In the spectrum of the pristine chitosan, some stretching vibrations were recorded at 3203, 2878, 1646, and 1030 cm^{-1} which attributed to the functional groups such as hydroxyl (–OH)/amine (–NH_2), aliphatic –CH (Al-CH), –NH, and –C–O–C, respectively [28]. According to the pure sodium alginate FT-IR spectrum, the transmittance values at 3260, 2914, 1590, 1406, and 1296 cm^{-1} were due to the stretching vibrations of –OH, Al–CH, symmetric carbonyl (sym –C═O), anti-symmetric carbonyl (a-sym –C═O), and carboxylate anion (–C═O–O), respectively [23,29]. In the spectrum of sodium alginate-iron oxide particles (SA_Fe), these stretching vibrations (–OH, Al-CH, sym –C═O, a-sym –C═O, and –C ═O–O) were recorded at 3355, 2914, 1590, 1406, and 1296 cm^{-1}, respectively. Furthermore, a peak was seen at 540 cm^{-1} due to the stretching vibration of Fe-O, and the presence of this vibration confirmed the formation of SA_Fe nanoparticles [30,31]. As seen in the FT-IR spectrum of chitosan nanoparticles without SA_Fe, –OH/–NH_2, Al–CH, –NH, and –C–O–C stretching vibrations were recorded at 3448, 2969, 1678, 1453, 1171, and 1059 cm^{-1}, respectively. Compared to the stretching vibrations of chitosan nanoparticles with the pure chitosan vibration, they were shifted to higher frequencies. This was attributed to the reaction conditions during the preparation of chitosan nanoparticles. As mentioned in the experimental section, the chitosan nanoparticles

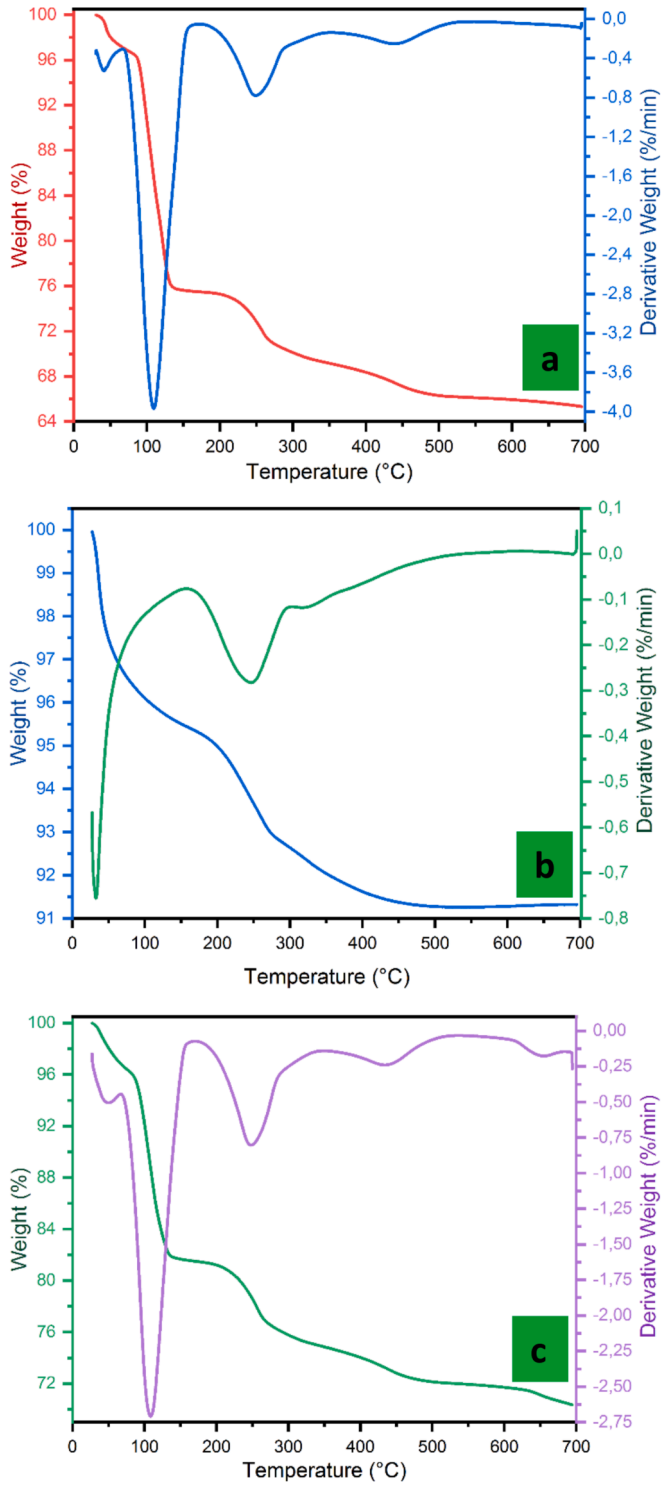

Fig. 5. TG-DTG curves of CS, SA_Fe, and CS@5.0SA_Fe nanoparticles.

were fabricated in an acidic medium. Mauricio-Sánchez and coworkers stated that FT-IR peaks shift to higher frequencies because of the protonation of chitosan in acidic media during the formation of chitosan nanoparticles [32]. In addition, a new peak was observed at 621 nm in the structure of chitosan nanoparticles due to the N–H/O–H wagging vibrations [33]. All stretching vibrations in the structure of the chitosan nanoparticles containing 2.5 %SA_Fe were seen at 3455, 2992, 1683, 1454, 1177, 1060, and 576 cm^{-1}, respectively. These results clearly indicated that the stretching vibrations of both chitosan and CS@SA_Fe nanoparticles were shifted to higher frequencies, and it was confirmed

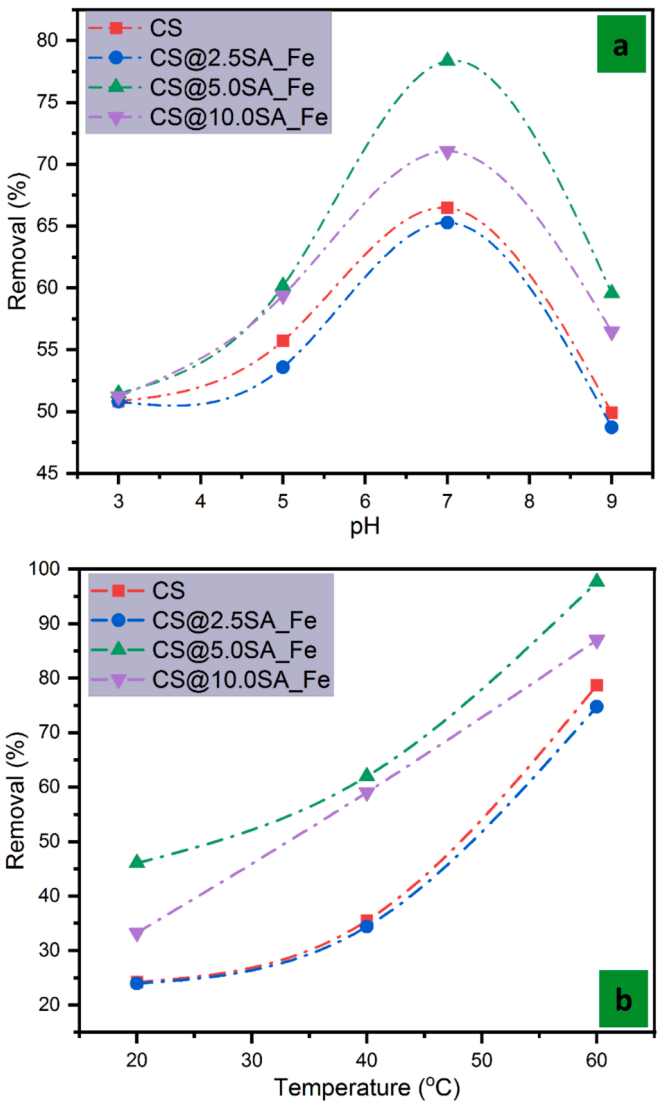

Fig. 6. Ph (a), and temperature (b) effect on the methylene blue adsorption.

that the successful preparation of the nanoparticles [34,35].

3.2. SEM analysis

Fig. 2 displays Scanning Electron Microscopy (SEM) images of SA_Fe, and chitosan nanoparticles containing 5.0 % SA_Fe. According to the SEM images of SA_Fe nanoparticles, it was composed of a homogenous and spherical morphology by the literature [36]. With the addition of SA_Fe nanoparticles into the chitosan matrix, the formation of nanorod-like structures was observed in the structure of the bioadsorbent. Moreover, spherical shapes in the structure of the nanorod-like structure of chitosan nanoparticles indicate the presence of sodium alginate-iron oxide nanoparticles [37].

3.3. XRD analysis

The crystalline nature of the SA_Fe, and 5.0 % SA_Fe containing chitosan nanoparticles (CS@5.0SA_Fe) were investigated by using an X-ray diffractometer (XRD), and XRD curves were given in Fig. 3. As clearly seen in Fig. 3, SA_Fe nanoparticles have 5 crystalline peaks at $2\theta = 30.3$, 35.6, 43.3, 57.2, and 63.0°, while SA_Fe containing CS nanoparticles have more multiple and sharp crystalline peaks at in the range from $2\theta = 19.9$ to 85.6°. The broad XRD peak at $2\theta = 20.31°$ indicated

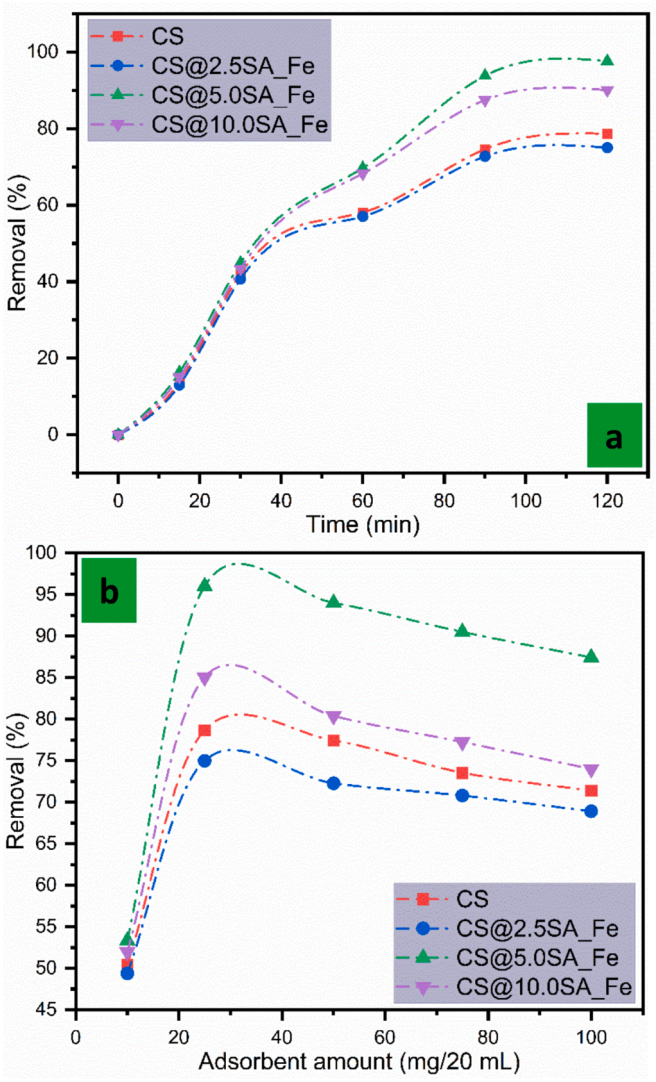

Fig. 7. Contact time (a), and bioadsorbent amount (b) effect on the methylene blue adsorption.

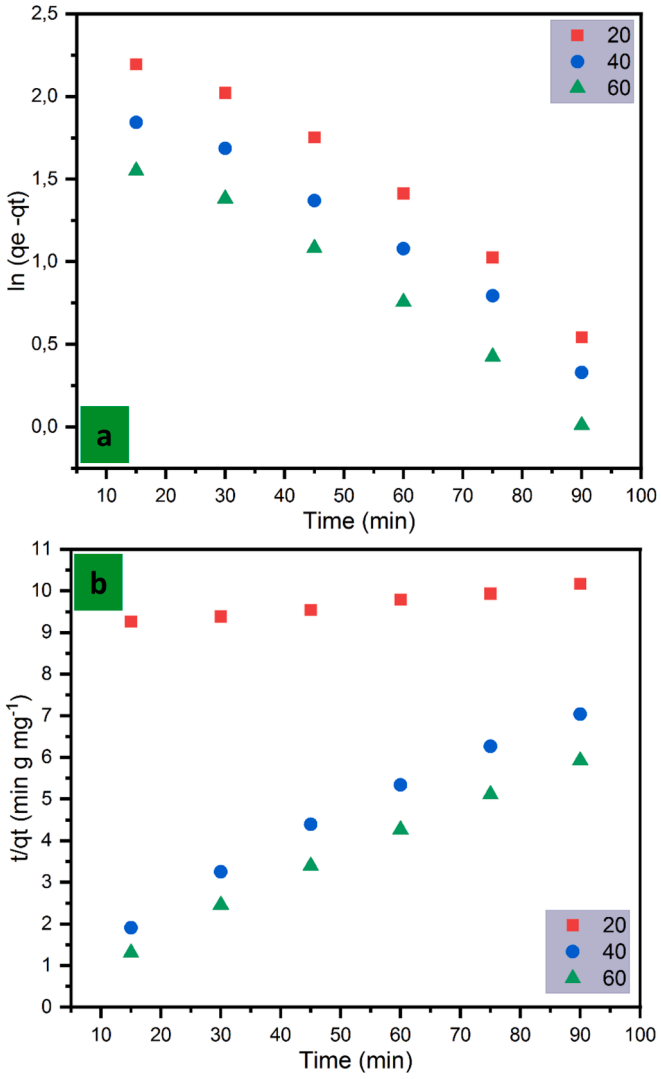

Fig. 8. Plots of pseudo-first-order (a), and second-order (b) for the adsorption of methylene blue of the bioadsorbents.

the presence of chitosan in the structure of CS@5.0SA_Fe [38]. According to the literature, sharp peaks around 35° confirmed that the iron oxide structure was formed in both sodium alginate and chitosan nanoparticle structures [39].

The particle size of SA-Fe and CS@5.0SA_Fe nanoparticles was calculated by using the XRD pattern of these nanomaterials and the Scherrer equation as follows:

$$D = \frac{0.89\lambda}{\beta cos\theta} \quad (9)$$

where λ is the wavelength (0.154 Å), θ is the Bragg diffraction angle, and β is the width at half maximum, respectively [40,41].

The findings indicated that the average nanoparticle size of the chitosan and SA_Fe nanoparticles was 10.64 ± 3.77 nm whereas it was determined as 18.73 ± 5.41 nm for the CS@5.0SA_Fe nanoparticles. This could be attributed to the presence of chitosan in the nanoparticle matrix. Sreekumar and coworkers stated that the particle size of the nanoparticles was increased with the addition of higher chitosan concentrations into the reaction medium [42].

3.4. BET analysis

The porous structure of the SA_Fe and chitosan-containing bioadsorbents were analyzed by using BET, and BJH. The nitrogen adsorption and desorption behavior of the SA_Fe, and the CS@5.0SA_Fe nanoparticles were shown in Fig. 4. The BET surface area and BJH diameter of the SA_Fe nanoparticles were found as 5.14 ± 0.023, and 5.80 $m^2 g^{-1}$, while they were detected as 7.29 ± 0.035, and 10.36 $m^2 g^{-1}$ for CS@5.0SA_Fe nanoparticles, respectively. The surface area and average diameter of CS@5.0SA_Fe nanoparticles were increased with the addition of SA-Fe nanoparticles into the chitosan solution. The pore volume and average pore diameter were also determined as 0.0021 $cm^3 g^{-1}$, and 1.05 nm for SA_Fe nanoparticles, and 0.0033 $cm^3 g^{-1}$, and 1.28 nm for CS@5.0SA_Fe nanoparticles, respectively.

3.5. Thermogravimetric analysis

The thermal stability of the fabricated bioadsorbents was clarified by using the TGA measurements (Fig. 5), and thermal behavior was evaluated in terms of char residue at 700 °C, 20 %, and 50 % weight loss. As can be seen in the thermogram of the bioadsorbents, SA_Fe nanoparticles were decomposed in two-step whereas CS, CS@2.5SA_Fe, CS@5.0SA_Fe, and CS@10.0SA_Fe were exhibited in three-step degradation behavior. The first and second degradation steps of SA_Fe were carried out in the range of 20 to 300 °C with 7.4 % weight loss, and 300 to 700 °C with 1.3 % weight loss due to evaporation of water molecules with physically

Table 1
Kinetic parameters for the adsorption of methylene blue onto the adsorbents (pH 7.0, and bioadsorbent amount: 10 mg).

Adsorbent	Temperature (°C)	First order			Second order		
		k_1 (min^{-1})	qe (mg g^{-1})	R^2	k_2 (g mg^{-1} min^{-1})	qe (mg g^{-1})	R^2
CS	20	0.0178	7.59	0.9884	0.0902	16.72	0.9955
CS@2.5SA_Fe		0.0203	6.60	0.9866	0.1152	16.09	0.9912
CS@5.0SA_Fe		0.0220	10.57	0.9758	0.0123	25.63	0.9904
CS@10.0SA_Fe		0.0261	9.58	0.9617	0.0172	22.76	0.9923
CS		0.0188	9.68	0.9877	0.0968	18.25	0.9902
CS@2.5SA_Fe	40	0.0147	9.67	0.9884	0.1044	18.09	0.9906
CS@5.0SA_Fe		0.0201	14.18	0.9822	0.0679	27.92	0.9908
CS@10.0SA_Fe		0.0235	10.58	0.9793	0.0832	24.23	0.9922
CS	60	0.0296	12.23	0.9839	0.0755	20.45	0.9975
CS@2.5SA_Fe		0.0188	10.81	0.9748	0.0918	19.95	0.9957
CS@5.0SA_Fe		0.0207	16.21	0.9862	0.0608	29.44	0.9961
CS@10.0SA_Fe		0.0275	13.03	0.9808	0.0713	24.69	0.9955

bounded structure, the degradation of iron oxide, and hydroxyl (–OH) and carboxyl (−C═O) groups of sodium alginate, and carbonization [29,43,44]. The three degradation steps of the bioadsorbents were observed in the range from 20 to 170 °C around 18.0 % weight loss, 170 to 330 °C around 7.0 % weight loss, and 330 to 700 °C around 5.0 % weight loss due to the evaporation of water, degradation of –OH and −C═O in the structure of chitosan and sodium alginate, and carbonization [43,45]. Furthermore, the char residue of the SA_Fe nanoparticles was recorded as 91.3 %. The T20 and char residue at 700 °C of chitosan nanoparticles were determined as 121 °C and 65.3 %. These values were recorded for the bioadsorbents in the range from 232 to 236 °C, and 70.4 to 71.2 %. These results clearly showed that with the addition of SA_Fe nanoparticles into the chitosan matrix, thermal stability (T20, and char) was increased.

3.6. Dye adsorption studies, and optimization

The methylene blue adsorption behavior of the chitosan and sodium alginate-based bioadsorbents was optimized concerning temperature, pH, bioadsorbent amounts, dye concentration, and contact time. These batch experiments were carried out at 25 °C, pH 7.0, and 20 mg L^{-1} dye concentration for 2 h in the presence of 20 mg bioadsorbent unless otherwise stated.

3.6.1. pH effect

The initial pH solution value has an important effect as it affects the charge of the adsorbent and the degree of ionization in the dye adsorption process [46]. With this aim, the pH effect on the methylene blue adsorption capacity of the bioadsorbent was studied in the range from pH 3.0 to 9.0. The pH value of the solutions was adjusted using 0.1 M HCl or 0.1 M NaOH (Fig. 6a). The methylene blue adsorption capacity of the bioadsorbents was calculated to be almost the same value (around 51 %) at low pH, and this removal value increased with the increasing of pH between 5 and 7. In the alkaline media, the dye removal capacity of the bioadsorbents was also decreased. At high pH values (in an alkaline environment) the amino groups of chitosan polymer remain in the form of $–NH_2$, which makes chitosan insoluble and the interaction of methylene blue molecules with chitosan decreases. Therefore, chitosan-based nanomaterials exhibited low dye adsorption behavior in alkaline environments [47].

Moreover, CS@5.0SA_Fe has the highest methylene blue adsorption capacity in the tested pH solution.

3.6.2. Temperature effect

Fig. 6b shows the effect of temperature on the adsorption capacity of methylene blue into bioadsorbents. According to Fig. 6b, the methylene blue removal capacity of the bioadsorbents was increased with the increasing temperature. This could be probably due to the adsorption reaction occurring kinetically faster with the increasing temperature and, therefore, the adsorption process of the methylene blue molecules onto the bioadsorbents carried out in lower equilibrium times [48]. Moreover, an increase in the temperature may increase the ionization of some functional groups such as −C = O, and –OH in the structure of chitosan and sodium alginate [23].

3.6.3. Contact time

The contact time effect on the methylene blue adsorption capacity of the bioadsorbents was given in Fig. 7a. The dye removal rate of all bioadsorbents increased linearly and reached around 40 % removal capacity within the first 30 min. The maximum methylene blue removal rate was obtained after 120 min, and they almost reached equilibrium at the mentioned time. In addition, the biosorbents exhibited a rapid cationic dye adsorption behavior. This could be attributed to the strong electrostatic interaction between the bioadsorbents and methylene blue molecules [49].

3.6.4. Bioadsorbent amount

To determine the bioadsorbent amount effect on the methylene blue removal behavior, the bioadsorbent amounts were increased from 10 to 100 mg (Fig. 7b). The maximum methylene blue removal rate was found to be 78.66, 54.98, 97.64, and 80.05 for CS, CS@2.5SA-Fe, CS@5.0SA-Fe, and CS@10.0SA-Fe in the presence of 25 mg bioadsorbents. Furthermore, the methylene blue adsorption behavior of the bioadsorbents decreased in the presence of 50, 75, and 100 mg adsorbent doses due to the limited active adsorption sites on the surface of the bioadsorbents [50]. According to the optimization results, 5 CS@5.0SA_Fe exhibited the highest adsorption capacity due to its surface area and active size.

3.7. Adsorption kinetics

The pseudo-first-order (PFO), and pseudo-second-order (PSO) kinetic models were used to evaluate the methylene blue adsorption rate of the bioadsorbents (Fig. 8, and Table 1). As known, adsorption kinetic studies are critical in dye or heavy metal adsorption experiments as they provide information about the system's equilibrium state [51]. K_1 (the rate constant for the PFO model), and qe (dye equilibrium adsorption capacity) values were calculated in the range from 0.0178 to 0.0220 min^{-1}, and 6.60 to 10.57 mg g^{-1} at 20 °C, 0.0188 to 0.0235 min^{-1}, and 9.67 to 14.18 mg g^{-1} at 40 °C, and 0.0188 to 0.0296 min^{-1}, and 10.81 to 16.21 mg g^{-1} at 60 °C. k_2 (the rate constant for the PSO model), and qe value were found in the range from 0.0123 to 0.1152 g mg^{-1} min^{-1}, and 16.09 to 29.44 mg g^{-1}, respectively. Also, the correlation coefficient (R^2) was determined between 0.9617, and 0.9884 for the PFO model, and 0.9902 and 0.9975 for the PSO model, respectively. These findings indicated that the highest R^2 values were obtained for the PSO model,

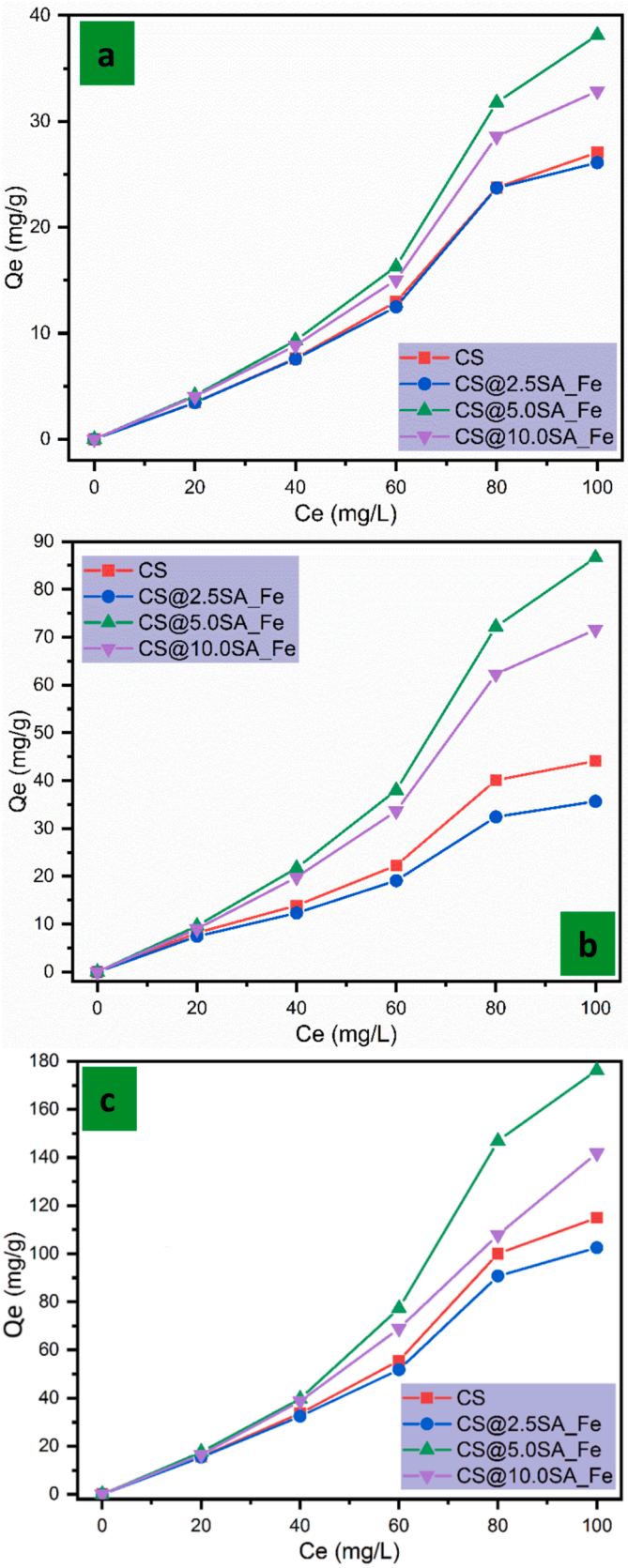

Fig. 9. Adsorption isotherm of the bioadsorbents at different temperatures such as 20 (a), 40 (b), and 60 °C (c).

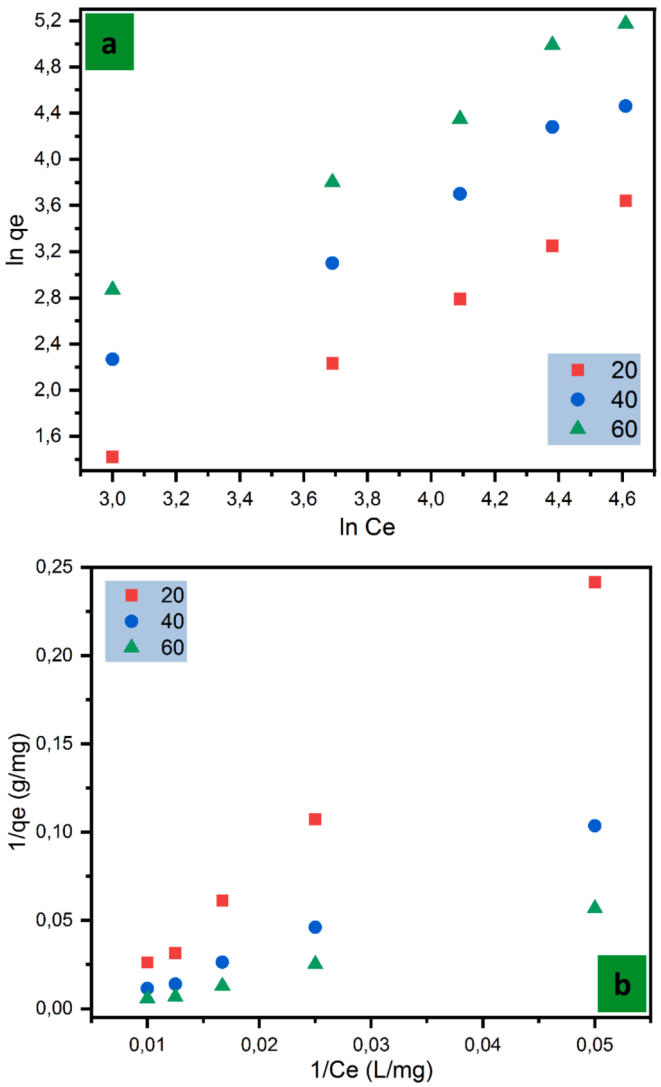

Fig. 10. Plots for Freundlich (a), and Langmuir for the adsorption of methylene blue.

and these experimental results were fitted with this kinetic model.

3.8. Adsorption isotherms

Methylene blue adsorption isotherm of the bioadsorbents was studied at various temperatures such as 20, 40, and 60 °C in the presence of 10 mg bioadsorbents and at pH 7.0 (Fig. 9). The methylene blue adsorption capacities of the bioadsorbents were calculated in the range from 26.10 to 38.14 mg/g at 20 °C, 35.68 to 86.63 mg/g at 40 °C, and 102.52 to 176.26 mg/g at 60 °C. According to these results, the methylene blue adsorption capacity of the bioadsorbents was increased with the increase in temperature. Arnata and coworkers explained that the increasing temperature of the reaction medium causes changes in the pore size of the adsorbents, the kinetic energy of the dye molecules, and an increase in the diffusion rate in dye adsorption studies [52].

Although investigating the adsorption behavior of bioadsorbents using adsorption models such as Langmuir and Freundlich is a basic approach, the obtained experimental results are very useful in providing information about adsorption mechanisms and capacities [53]. For this purpose, linear or nonlinear isotherm models of Langmuir and Freundlich of the bioadsorbents were given in Fig. 10, and results were shown in Table 2. Freundlich adsorption constant (K_F) was determined in the range from 26.10 to 27.44 mg g^{-1} (L mg^{-1})$^{1/n}$, 9.48 to 20.07 mg g^{-1} (L

Table 2
Isotherm model results for the adsorption of methylene blue onto the bioadsorbents (pH 7.0, and bioadsorbent amount: 10 mg).

Adsorbent	Temperature (°C)	Freundlich model			Langmuir model		
		K_F (mg g^{-1}) (L mg^{-1})$^{1/n}$	1/n	R^2	qmax (mg g^{-1})	K_L (L mg^{-1})	R^2
CS	20	26.37	1.28	0.9875	33.23	6.40	0.9984
CS@2.5SA_Fe		26.10	1.27	0.9839	32.26	6.43	0.9978
CS@5.0SA_Fe		27.44	1.37	0.9851	41.95	5.47	0.9985
CS@10.0SA_Fe		27.29	1.35	0.9852	35.71	5.55	0.9982
CS	40	14.06	1.05	0.9676	58.80	2.52	0.9929
CS@2.5SA_Fe		9.48	0.94	0.9706	50.05	2.68	0.9952
CS@5.0SA_Fe		20.07	1.41	0.9833	86.34	2.34	0.9987
CS@10.0SA_Fe		18.59	1.34	0.9870	82.65	2.47	0.9984
CS	60	10.88	1.35	0.9878	169.49	1.39	0.9982
CS@2.5SA_Fe		8.38	1.22	0.9882	162.77	1.40	0.9979
CS@5.0SA_Fe		15.72	1.47	0.9862	212.77	1.31	0.9981
CS@10.0SA_Fe		11.93	1.31	0.9860	204.08	1.34	0.9921

Table 3
The maximum adsorption capacities of bioadsorbents containing chitosan, and sodium alginate.

Bioadsorbent content	q_{max} (mg/g)	Reference
Cellulose nanofiber, and chitosan	164.5	43
Chitosan, iron, and silver nanoparticles	74.63	47
Cellulose, sodium alginate, and iron	105.93	48
Iron, chitosan, and SBA-15	176.70	49
Sodium alginate, zeolite, and iron	181.85	50
Chitosan and sodium alginate-iron	212.77	This study

Table 4
Thermodynamic data of the bioadsorbents.

Adsorbent	Temperature (K)	ΔG^o (kJ/mol)	ΔH^o (kJ/mol)	ΔS^o (kJ mol^{-1} K^{-1})	R^2
CS	293	−4.524	−31.100	−90.963	0.9919
	313	−2.406			
	333	−0.912			
CS@2.5SA_Fe	293	−4.536	−31.064	−90.839	0.9897
	313	−2.381			
	333	−0.932			
CS@5.0SA_Fe	293	−4.142	−29.089	−85.335	0.9949
	313	−2.213			
	333	−0.748			
CS@10.0SA_Fe	293	−4.177	−28.894	−84.454	0.9981
	313	−2.354			
	333	−0.811			

$mg^{-1})^{1/n}$, and 8.38 to 15.72 mg g^{-1} (L $mg^{-1})^{1/n}$ for 20, 40, and 60 °C, respectively. In addition, R^2 values for Freundlich isotherm was found between 0.9676 and 0.9882. According to the obtained results from Langmuir, Langmuir adsorption capacity and R^2 were calculated in the range from 1.31 to 6.41 L mg^{-1}, and 0.9921 to 0.9987. As can be seen in these results, the experimental results were fitted with Langmuir isotherm because the calculated R^2 values were higher than the other isotherm model and they were close to 1 [54].

The maximum methylene blue adsorption capacities of the chitosan and sodium alginate-iron oxide nanoparticles containing bioadsorbents were compared with the previous papers in the literature, and the findings were summarized in Table 3 [44,50,55–57]. The results indicated that the q_{max} value for the present study was higher than the other experimental results, and the fabricated bioadsorbents were competitive for the adsorption of methylene blue in the aqueous solutions.

3.9. Thermodynamic parameters

The thermodynamic parameters such as Gibbs free energy (G^o), enthalpy (H^o), and entropy (S^o) are very important as they provide information about whether the adsorption process will be endothermic or exothermic and whether it will occur spontaneously or not [58]. These adsorption thermodynamic parameters were calculated using different temperatures such as 293, 313, and 333 K (Table 4). ΔG^o values of the bioadsorbents were found between – 4.536 and – 0.748 kJ mol^{-1}. ΔH^o, and ΔS^o values of the CS, CS@2.5SA_Fe, CS@5.0SA_Fe, and CS@10.0SA_Fe were determined as – 31.100 kJ mol^{-1}, and – 90.963 kJ mol^{-1} K^{-1}, – 31.064 kJ mol^{-1}, and – 90.839 kJ mol^{-1} K^{-1}, – 29.089 kJ mol^{-1}, and – 85.335 kJ mol^{-1} K^{-1}, and – 28.894 kJ mol^{-1}, and – 84.454 kJ mol^{-1} K^{-1}, respectively. These results showed that the methylene blue adsorption process onto the bioadsorbents was carried out via spontaneous and exothermic reactions due to negative values of ΔG^o, and ΔH^o [59]. The negative value of ΔG^o showed that bioadsorbents tended to have more methylene blue adsorption behavior in the aqueous solution compared to the non-spontaneous reaction [58]. Moreover, the bioadsorbents and methylene blue molecules interacted with each other via electrostatic interactions, hydrogen bonding, or van der Waals due to the negative value of ΔS^o [23,60]. According to these findings, the possible interaction mechanism between the bioadsorbents and methylene blue molecules was given in Fig. 11.

FT-IR spectra of CS@5.0SA_Fe bioadsorbent in the presence and absence of methylene blue were given in Fig. 12 to confirm the interaction between dye molecules and bioadsorbents. The characteristic stretching vibrations such as hydroxyl (–OH)/amine, aliphatic –CH, –NH, symmetric −C = O, anti-symmetric −C = O, carboxylate anion (−C = O-O), and −C-O-C were observed at 3454, 2938, 1681, 1452, 1057, 847, and 562 cm^{-1} for the CS@5.0SA_Fe. When mixed biosorbent with dye molecules, these mentioned stretching vibrations were seen at 3308, 2885, 1637, 1367, 1052, 894 (as a shoulder) and 662 (as a shoulder) cm^{-1} for CS@5.0SA_Fe-dye mixture, respectively.

3.10. Regeneration of the bioadsorbents, and ion leaching effect

To determine the adsorption/desorption behavior of CS@5.0SA_Fe nanoparticles, 5 consecutive experiments were performed, and the results were given in Fig. 13a. It was found that a decrease of around 15 % was found after 5 consecutive adsorption/desorption cycles. According to these results, the fabricated bioadsorbents could be effectively used for the adsorption of methylene blue from wastewater.

To investigate the stability of the CS@5.0SA_Fe nanoparticles, ion leaching studies were done in the presence of 20 mg bioadsorbents, 20 mg/L methylene blue, and at pH 5.0, 7.0, and 9.0 under ambient conditions (Fig. 13b). The finding showed that the ion leaching effect of the tested ions on CS@5.0SA_Fe nanoparticles was lower than 5 μg/L. According to these results, it was found that the leaching effect of tested metal ions during the adsorption process was insignificant and the CS@5.0SA_Fe nanoparticles exhibited quite high stability in a wide pH

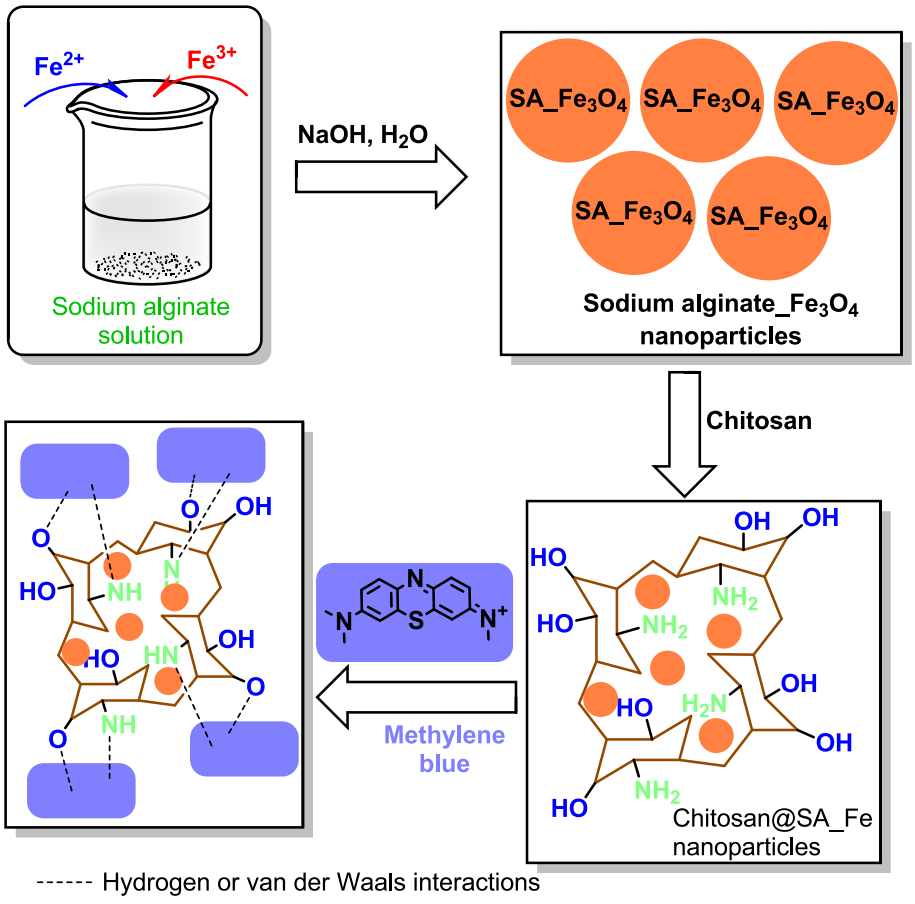

Fig. 11. Possible adsorption mechanism.

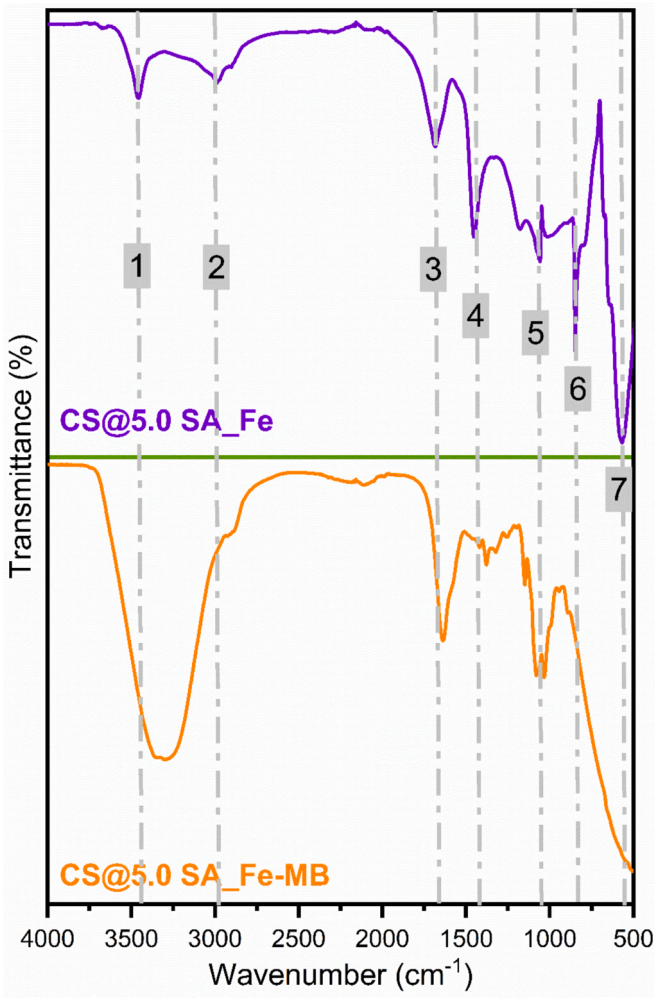

Fig. 12. FT-IR spectra of chitosan nanoparticles containing 5.0 % sodium alginate-iron nanoparticles (CS@SA_Fe) before and after adsorption of dye. (Stretching vibrations = 1: hydroxyl (–OH)/amine (–NH_2), 2: aliphatic –CH, 3: –NH, 4: symmetric –C═O, 5: anti-symmetric –C═O, 6: carboxylate anion (–C═O-O), and 7: –C–O–C).

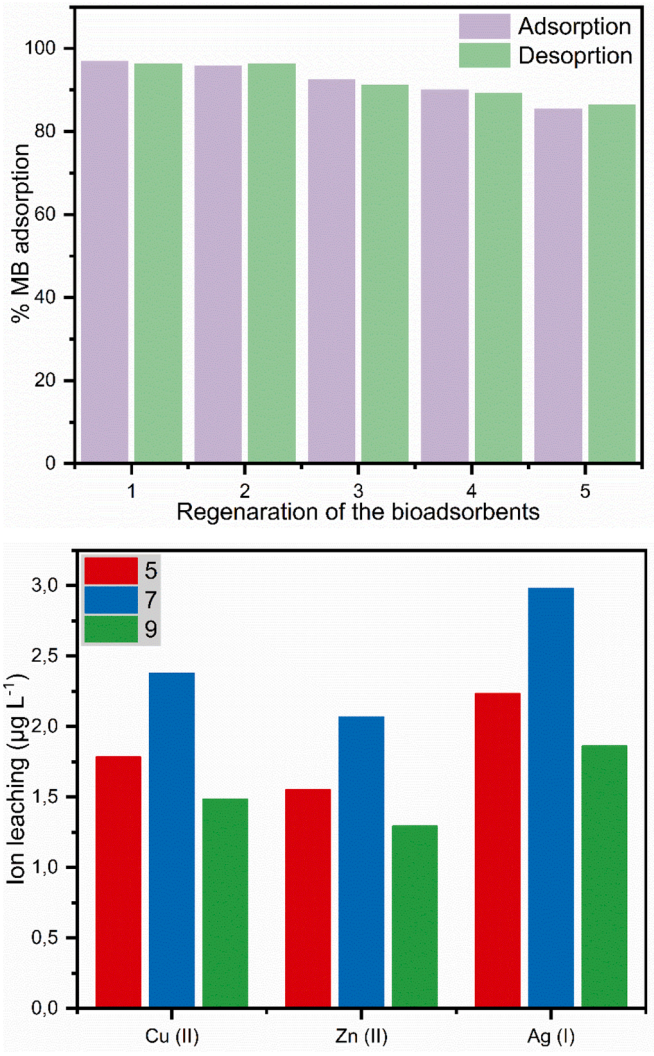

Fig. 13. Regeneration of methylene blue onto the chitosan and sodium alginate-iron oxide nanoparticles (a), and ion leaching effect on the CS@5.0SA_Fe (b) at different pH values.

range [61–63].

4. Conclusion

In the present paper, a series of bioadsorbents containing chitosan, and sodium alginate-iron oxide nanoparticles were successfully prepared to remove methylene blue from the aqueous solution. Sodium alginate-iron oxide particle was obtained and mixed with chitosan due to the increased surface area of the chitosan, and the enhanced adsorption behavior of the bioadsorbents. As known, biopolymers such as chitosan and sodium alginate-based bioadsorbent are more advantageous than synthetic polymer-based adsorbents in terms of environmental and economic sustainability due to their biodegradable and low-cost properties. The average particle size of the SA_Fe and CS@5.0SA_Fe was found to be 10.64 ± 3.77, and 18.73 ± 5.41 nm. The methylene blue adsorption behavior of the bioadsorbents was optimized in terms of pH, temperature, contact time, and bioadsorbent amount. The findings showed that CS@5.0SA_Fe exhibited maximum methylene blue adsorption behavior in all tested conditions due to its high surface area and active size. Kinetic and isotherm adsorption models were also investigated, and methylene blue adsorption of the bioadsorbents was fitted with the pseudo-second kinetic and Langmuir isotherm model. Maximum methylene blue capacity was found to be 212.77 mg g^{-1} in the presence of 10 mg CS@5.0SA_Fe at 60 °C, and pH 7.0.

CRediT authorship contribution statement

Umran Duru Kamaci: Writing – review & editing, Investigation, Formal analysis, Conceptualization. **Musa Kamaci:** Writing – review & editing, Writing – original draft, Validation, Methodology.

Declaration of competing interest

The authors declare that they have no known competing financial interests or personal relationships that could have appeared to influence the work reported in this paper.

Data availability

Data will be made available on request.

References

[1] Y. Rashtbari, F. Sher, S. Afshin, A. Hamzezadeh, S. Ahmadi, O. Azhar, A. Rastegar, S. Ghosh, Y. Poureshgh, Green synthesis of zero-valent iron nanoparticles and loading effect on activated carbon for furfural adsorption, Chemosphere 287 (2022) 132114, https://doi.org/10.1016/j.chemosphere.2021.132114.

[2] C. Osagie, A. Othmani, S. Ghosh, A. Malloum, Z.K. Esfahani, S. Ahmadi, Dyes adsorption from aqueous media through the nanotechnology: A review, J. Mater. Res. Technol. 14 (2021) 2195–2218, https://doi.org/10.1016/j.jmrt.2021.07.085.
[3] T.A. Aragaw, F.M. Bogale, B.A. Aragaw, Iron-based nanoparticles in wastewater treatment: A review on synthesis methods, applications, and removal mechanisms, J. Saudi Chem. Soc. 25 (2021) 101280, https://doi.org/10.1016/j.jscs.2021.101280.
[4] D. Uzunoglu, A. Ozer, Facile Synthesis of magnetic iron-based nanoparticles from the leach solution of hyperaccumulator plant pinus brutia for the antibacterial activity and colorimetric detection of ascorbic acid, ACS Appl. Bio Mater. 5 (2022) 5465–5476, https://doi.org/10.1021/acsabm.2c00782.
[5] G.T. Tee, X.Y. Gok, W.F. Yong, Adsorption of pollutants in wastewater via biosorbents, nanoparticles and magnetic biosorbents: A review, Environ. Res. 212 (2022) 113248, https://doi.org/10.1016/j.envres.2022.113248.
[6] A. Yao, Y. Wang, J. Yu, S. Tian, Y. Zhan, H. Liao, J. Lan, S. Lin, Fe-pillared montmorillonite functionalized chitosan/gelatin foams for efficient removal of organic pollutants by integration of adsorption and Fenton degradation, Carbohydr. Polym. 321 (2023) 121265, https://doi.org/10.1016/j.carbpol.2023.121265.
[7] A. Mokhtari, M. Sabzi, H. Azimi, 3D porous bioadsorbents based on chitosan/alginate/cellulose nanofibers as efficient and recyclable adsorbents of anionic dye, Carbohydr. Polym. 265 (2021) 118075, https://doi.org/10.1016/j.carbpol.2021.118075.
[8] C. Zhang, A. Yao, J. Lan, B. Dou, L. Yang, S. Lin, Fabrication of poly(itaconic acid)-*g*-potassium alginate aerogels as eco-friendly biosorbents for removal of cationic dyes, J. Macromol. Sci. Part A 60 (2023) 231–245, https://doi.org/10.1080/10601325.2022.2140674.
[9] U. Duru Kamaci, A. Peksel, Fabrication of PVA-chitosan-based nanofibers for phytase immobilization to enhance enzymatic activity, Int. J. Biol. Macromol. 164 (2020) 3315–3322, https://doi.org/10.1016/j.ijbiomac.2020.08.226.
[10] P. Bhatt, S. Joshi, G.M.U. Bayram, P. Khati, H. Simsek, Developments and application of chitosan-based adsorbents for wastewater treatments, Environ. Res. 226 (2023) 115530, https://doi.org/10.1016/j.envres.2023.115530.
[11] U. Duru Kamaci, M. Kamaci, Preparation of polyvinyl alcohol, chitosan and polyurethane-based pH-sensitive and biodegradable hydrogels for controlled drug release applications, Int. J. Polym. Mater. Polym. Biomater. 69 (2020) 1167–1177, https://doi.org/10.1080/00914037.2019.1670180.
[12] A.K. Mallik, S.M.F. Kabir, F.B. Abdur Rahman, M.N. Sakib, S.S. Efty, M.M. Rahman, Cu(II) removal from wastewater using chitosan-based adsorbents: A review, J. Environ. Chem. Eng. 10 (2022) 108048, Doi: 10.1016/j.jece.2022.108048.
[13] A.M. Elgarahy, K.Z. Elwakeel, S.H. Mohammad, G.A. Elshoubaky, A critical review of biosorption of dyes, heavy metals and metalloids from wastewater as an efficient and green process, Clean. Eng. Technol. 4 (2021) 100209, https://doi.org/10.1016/j.clet.2021.100209.
[14] M. Kamaci, I. Kaya, Preparation of biodegradable, and pH-sensitive poly (azomethine)-chitosan hydrogels for potential application of 5-fluoro uracil delivery, Eur. Polym. J. 158 (2021) 110680, https://doi.org/10.1016/j.eurpolymj.2021.110680.
[15] A.M. Omer, R. Dey, A. S. Eltaweil, E. M. Abd El-Monaem, Z.M. Ziora, Insights into recent advances of chitosan-based adsorbents for sustainable removal of heavy metals and anions, Arab. J. Chem.15 (2022) 103543, Doi: 10.1016/j.arabjc.2021.103543.
[16] A.A. El-Bindary, A.Z. El-Sonbati, A.A. Al-Sarawy, K.S. Mohamed, M.A. Farid, Adsorption and thermodynamic studies of hazardous azocoumarin dye from an aqueous solution onto low cost rice straw based carbons, J. Mol. Liq. 199 (2014) 71–78, https://doi.org/10.1016/j.molliq.2014.08.010.
[17] G.A.A. Al-Hazmi, A.A. El-Zahhar, M.G. El-Desouky, M.A. El-Bindary, A.A. El-Bindary, Efficiency of Fe_3O_4@ZIF-8 for the removal of doxorubicin from aqueous solutions: Equilibrium, kinetics and thermodynamic studies, Environ. Technol. 45 (2022) 731–750, https://doi.org/10.1080/09593330.2022.2121181.
[18] A.M. Alsuhaibani, A.A.A. Alayyafi, L.A. Albedair, M.G. El-Desouky, A.A. El-Bindary, Synthesis and characterization of metal–organic frameworks based on thorium for the effective removal of 2,4-dichlorophenylacetic pesticide from water: Batch adsorption and Box-Behnken design optimization, and evaluation of reusability, J. Mol. Liq. 398 (2024) 124252, https://doi.org/10.1016/j.molliq.2024.124252.
[19] M. Buzga, E. Machytka, E. Dvorackova, Z. Svagera, D. Stejskal, J. Maca, J. Kral, Methylene blue: A controversial diagnostic acid and medication? Toxicol. Res. 11 (2022) 711–717, https://doi.org/10.1093/toxres/tfac050.
[20] J.F. Lutz, S. Stiller, A. Hoth, L. Kaufner, U. Pison, R. Cartier, One-pot synthesis of PEGylated ultrasmall iron-oxide nanoparticles and their in vivo evaluation as magnetic resonance imaging contrast agents, Biomacromolecules 7 (2006) 3132–3138, https://doi.org/10.1021/bm0607527.
[21] H. Huang, Q. Yang, L. Zhang, C. Huang, Y. Liang, Polyacrylamide modified kaolin enhances adsorption of sodium alginate/carboxymethyl chitosan hydrogel beads for copper ions, Chem. Eng. Res. Des. 180 (2022) 296–305, https://doi.org/10.1016/j.cherd.2022.02.030.
[22] M. Kamaci, I. Kaya, Fabrication of biodegradable hydrogels based on chitosan and poly(azomethine-urethane) containing phenyl triazine for drug delivery, Polym. Adv. Technol. 33 (2022) 2645–2655, https://doi.org/10.1002/pat.5720.
[23] U. Duru Kamaci, M. Kamaci, Hydrogel beads based on sodium alginate and quince seed nanoparticles for the adsorption of methylene blue, Inorg. Chem. Commun. 160 (2024) 111919, https://doi.org/10.1016/j.inoche.2023.111919.
[24] L. Wu, S. Qi, T. Zhang, Y. Jin, H. Xiao, One-step carbonization/activation synthesis of chitosan-based porous sheet-like carbon and studies of adsorptive removal for Rhodamine B, Carbohydr. Polym. 330 (2024) 121832, https://doi.org/10.1016/j.carbpol.2024.121832.
[25] F. Abbasi, M. Mansouri, M. Tanzifi, F. Ebrahimi, A. Sadeghizadeh, The modified pomegranate peel as an economical and highly effective adsorbent for malachite green dye removal from wastewater, Coll. Surf. C Environ. Asp. 2 (2024) 100040, https://doi.org/10.1016/j.colsuc.2024.100040.
[26] H. Liu, B. Wang, H. Liu, Y. Zheng, M. Li, K. Tang, B. Pan, C. Liu, J. Luo, X. Pang, Multi-crosslinked robust alginate/polyethyleneimine modified graphene aerogel for efficient organic dye removal, Coll. Surf. A Physicochem. Eng. Asp. 683 (2024) 133034, https://doi.org/10.1016/j.colsurfa.2023.133034.
[27] L.H. Alfhaid, H.K. Alshammeri, S.S. Lahmadi, A.M. Beagan, K.M. Alotaibi, M. S. Almeateq, A.M. Alswieleh, Effective and fast removal of ionic dyes from contaminated water using multi-walled carbon nanotubes decorated with polyelectrolyte brushes, Polym. Adv. Technol. 35 (2024) e6480.
[28] M. Kamaci, I. Kaya, Chitosan based hybrid hydrogels for drug delivery: Preparation, biodegradation, thermal, and mechanical properties, Polym. Adv. Technol. 34 (2023) 779–788, https://doi.org/10.1002/pat.5930.
[29] U. Duru Kamaci, A. Peksel, Enhanced catalytic activity of immobilized phytase into polyvinyl alcohol-sodium alginate based electrospun nanofibers, Catal. Lett. 151 (2021) 821–831, https://doi.org/10.1007/s10562-020-03339-0.
[30] R. Jain, S. Mendiratta, L. Kumar, A. Srivastava, Green synthesis of iron nanoparticles using Artocarpus heterophyllus peel extract and their application as a heterogeneous Fenton-like catalyst for the degradation of Fuchsin Basic dye, Curr. Res. Green Sustain. Chem. 4 (2021) 100086, https://doi.org/10.1016/j.crgsc.2021.100086.
[31] U. Duru Kamaci, M. Kamaci, A. Peksel, A dual responsive colorimetric sensor based on polyazomethine and ascorbic acid for the detection of Al (III) and Fe (II) ions, Spectrochim. Acta A Mol. Biomol. Spectrosc. 254 (2021) 119650, https://doi.org/10.1016/j.saa.2021.119650.
[32] R.A. Mauricio-Sanchez, R. Salazar, J.G. Luna-Barcenas, A. Mendoza-Galvan, FTIR spectroscopy studies on the spontaneous neutralization of chitosan acetate films by moisture conditioning, Vib. Spectrosc 94 (2018) 1–6, https://doi.org/10.1016/j.vibspec.2017.10.005.
[33] I. Dziedzic, A. Kertmen, Methods of chitosan identification: History and trends, Lett. Appl. Nanobioscience 12 (2023) 94, https://doi.org/10.33263/LIANBS124.094.
[34] U. Duru Kamaci, M. Kamaci, Boric acid and Schiff base-based fluorescent sensor for detection of L-tryptophan in milk and BSA samples, Turk. J. Chem. 46 (2022) 27, Doi: 10.55730/1300-0527.3381.
[35] M. Kamacı, I. Kaya, Synthesis of metal-coordinated poly(azomethine-urethane)s: Thermal stability, optical and electrochemical properties, J. Inorg. Organomet. Polym. 23 (2013) 1159–1171, https://doi.org/10.1007/s10904-013-9908-8.
[36] S.S.U. Rahman, M.T. Qureshi, K. Sultana, W. Rehman, M.Y. Khan, M.H. Asif, M. Farooq, N. Sultana, Single step growth of iron oxide nanoparticles and their use as glucose biosensor, Results Phys. 7 (2017) 4451–4456, https://doi.org/10.1016/j.rinp.2017.11.001.
[37] M. Appu, Z. Lian, D. Zhao, J. Huang, Biosynthesis of chitosan–coated iron oxide (Fe_3O_4) hybrid nanocomposites from leaf extracts of Brassica oleracea L and study on their antibacterial potentials, 3 Biotech. 11 (2021) 271, Doi: 10.1007/s13205-021-02820-w.
[38] K. Lakkaboyana, K. Soontarapa, R.K. Vinaykumar, K.K. Marella, Preparation of novel chitosan polymeric nanocomposite as an efficient materials for the removal of acid blue 25 from aqueous environment, Int. J. Biol. Macromol. 168 (2021) 760–768, https://doi.org/10.1016/j.ijbiomac.2020.11.133.
[39] S. Nasiri, M. Rabiei, A. Palevicius, G. Janusas, A. Vilkauskas, V. Nutalapati, A. Monshi, Modified Scherrer equation to calculate crystal size by XRD with high accuracy, examples Fe_2O_3, TiO_2 and V_2O_5, Nano Trends 3 (2023) 100015, https://doi.org/10.1016/j.nwnano.2023.100015.
[40] U. Duru Kamaci, M. Kamaci, Selective and sensitive ZnO quantum dots based fluorescent biosensor for detection of cysteine, J. Fluoresc. 31 (2021) 401–414, https://doi.org/10.1007/s10895-020-02671-3.
[41] M. Kamaci, A polycaprolactone-capped ZnO quantum dots-based fluorometric sensor for the detection of Fe^{3+} ions in seawater, J. Fluoresc. 34 (2024) 1643–1654, https://doi.org/10.1007/s10895-023-03394-x.
[42] S. Sreekumar, F.M. Goycoolea, B.M. Moerschbacher, G.R. Rivera-Rodriguez, Parameters infuencing the size of chitosan-TPP nano- and microparticles, Sci. Rep. 8 (2018) 4695, https://doi.org/10.1038/s41598-018-23064-4.
[43] A. Avcı, M. Kamaci, I. Kaya, M. Yıldırım, Synthesis of novel crosslinked poly (azomethine-urethane)s: Photophysical and thermal properties, Mater. Chem. Phys. 163 (2015) 301–310, https://doi.org/10.1016/j.matchemphys.2015.07.044.
[44] Y. Fang, Q. Liu, S. Zhu, Selective biosorption mechanism of methylene blue by a novel and reusable sugar beet pulp cellulose/sodium alginate/iron hydroxide composite hydrogel, Int. J. Biol. Macromol. 188 (2021) 993–1002, https://doi.org/10.1016/j.ijbiomac.2021.07.192.
[45] I. Kaya, M. Yildirim, M. Kamaci, A. Avci, New poly(azomethine-urethane)s including melamine derivatives in the main chain: Synthesis and thermal characterization, J. Appl. Polym. Sci. 120 (2011) 3027–3035, https://doi.org/10.1002/app.33441.
[46] R. Ahmad, K. Ansari, Comparative study for adsorption of congo red and methylene blue dye on chitosan modified hybrid nanocomposite, Process Biochem. 108 (2021) 90–102, https://doi.org/10.1016/j.procbio.2021.05.013.
[47] S. Zhao, F. Zhou, L. Li, M. Cao, D. Zuo, H. Liu, Removal of anionic dyes from aqueous solutions by adsorption of chitosan-based semi-IPN hydrogel composites, Compos. B Eng. 43 (2012) 1570–1578, https://doi.org/10.1016/j.compositesb.2012.01.015.

[48] R. Khushbu, Jindal, Sodium alginate and chitosan-based amphoteric nanocomposites modified with graphene oxide and bentonite as an efficient adsorbent for both anionic and cationic dyes, J. Polym. Environ. 31 (2023) 264–286, https://doi.org/10.1007/s10924-022-02626-8.
[49] F. Wei, Y. Zhu, T. He, S. Zhu, T. Wang, C. Yao, C. Yu, P. Huang, Y. Li, Q. Zhao, W. Son, Insights into the pH-dependent adsorption behavior of ionic dyes on phosphoric acid-activated biochar, ACS Omega 7 (2022) 46288–46302, https://doi.org/10.1021/acsomega.2c04799.
[50] J. Qiu, P. Fan, Y. Feng, F. Liu, C. Ling, A. Li, Comparison of the adsorption behaviors for methylene blue on two renewable gels with different physical state, Environ. Pollut. 254 (2019) 113117, https://doi.org/10.1016/j.envpol.2019.113117.
[51] M.S. Kazemi, A. Sobhani, $CuMn_2O_4$/chitosan micro/nanocomposite: Green synthesis, methylene blue removal, and study of kinetic adsorption, adsorption isotherm experiments, mechanism and adsorbent capacity, Arab. J. Chem. 16 (2013) 104754, https://doi.org/10.1016/j.arabjc.2023.104754.
[52] I.W. Arnata, F. Suprihatin, N. Fahma, T.C. Richana, Sunarti, Adsorption of anionic congo red dye by using cellulose from sago frond, Poll. Res. 38 (2019) 557–567.
[53] K.A. Omran, M.R. El-Aassar, O.M. Ibrahim, S.A. Sharaewy, R.E. Khalifa, F. M. Mohamed, Chitosan/alginate nanocomposites containing magnetic nanoparticles and multi-wall carbon nanotubes for efficient iron sorption, Desalin. Water Treat. 317 (2024) 100294, https://doi.org/10.1016/j.dwt.2024.100294.
[54] L. Yang, Y. Zhan, R. Yu, J. Lan, J. Shang, B. Dou, H. Liu, R. Zou, S. Lin, Facile and scalable fabrication of antibacterial CO_2–responsive cotton for ultrafast and controllable removal of anionic dyes, ACS Appl. Mater. Interfaces 13 (2021) 2694–2709, https://doi.org/10.1021/acsami.0c19750.
[55] R.D. Ningtyas, D.D. Yanti, A.K. Amin, A. Aji, Fabrication of a Fe_3O_4/CS/AgNPs composite from indigenous iron sand for enhanced methylene blue adsorption, J. Clust. Sci. 35 (2024) 1463–1480, https://doi.org/10.1007/s10876-024-02594-0.
[56] T. Meechai, T. Poonsawat, N. Limchoowong, S. Laksee, P. Chumkaeo, R. Tuanudom, A. Yatsomboon, L. Honghernsthit, E. Somsook, P. Sricharoen, One-pot synthesis of iron oxide-Gamma irradiated chitosan modified SBA-15 mesoporous silica for effective methylene blue dye removal, Heliyon 9 (2023) e16178, https://doi.org/10.1016/j.heliyon.2023.e16178.
[57] F. Liu, W. Li, Y. Zhou, Preparation and characterization of magnetic sodium alginate-modified zeolite for the efficient removal of methylene blue, Coll. Surf. A Physicochem. Eng. Asp. 629 (2021) 127403, https://doi.org/10.1016/j.colsurfa.2021.127403.
[58] J. Kazemi, V. Javanbakht, Alginate beads impregnated with magnetic chitosan@zeolite nanocomposite for cationic methylene blue dye removal from aqueous solution, Int. J. Biol. Macromol.1 154 (2020) 1421437, https://doi.org/10.1016/j.ijbiomac.2019.11.024.
[59] E. Alver, A.U. Metin, F. Brouers, Methylene blue adsorption on magnetic alginate/rice husk bio-composite, Int. J. Biol. Macromol. 154 (2020) 104–113, https://doi.org/10.1016/j.ijbiomac.2020.02.330.
[60] J. Yu, S. Tian, A. Yao, H. Hu, J. Lan, L. Yang, X. Du, S. Lin, Compressible polydopamine modified pomelo peel powder/poly (ethyleneimine)/κ-carrageenan aerogel with pH-tunable charge for selective removal of anionic and cationic dyes, Carbohydr. Polym. 323 (2024) 121377, https://doi.org/10.1016/j.carbpol.2023.121377.
[61] H.A. Kiwaan, F.S. Mohamed, N.A. El-Ghamaz, N.M. Beshry, A.A. El-Bindary, Experimental and electrical studies of zeolitic imidazolate framework-8 for the adsorption of different dyes, J. Mol. Liq. 338 (2021) 116670, https://doi.org/10.1016/j.molliq.2021.116670.
[62] G.A.A.M. Al-Hazmi, A.A.A. Alayyafi, M.G. El-Desouky, A.A. El-Bindary, Guava seed activated carbon loaded calcium alginate aerogel for the adsorption of diclofenac sodium: Characterization, isotherm, kinetics, and optimization via Box-Behnken design, Int. J. Biol. Macromol. 262 (2024) 129995, https://doi.org/10.1016/j.ijbiomac.2024.129995.
[63] G.A.A.M. Al-Hazmi, A.A.A. Alayyafi, M.G. El-Desouky, A.A. El-Bindary, Chitosan-nano CuO composite for removal of mercury (II): Box-Behnken design optimization and adsorption mechanism, Int. J. Biol. Macromol. 261 (2024) 129769, https://doi.org/10.1016/j.ijbiomac.2024.129769.

Umran Duru Kamaci is a part of the Department of Chemistry at Yildiz Technical University in Turkey. Her research focuses on biomaterials, nano-biocomposites, enzyme technology, drug delivery, and biosensors.

Musa Kamaci is an Associate Professor at Piri Reis University, Turkey. His research areas include nanomaterials for dye adsorption, hydrogels for drug delivery systems, polymers, fluorescent sensors, and polymeric materials.